Continental Shelf Research 43 (2012) 10–23

Contents lists available at SciVerse ScienceDirect

Continental Shelf Research

journal homepage: www.elsevier.com/locate/csr

Research papers

The morphodynamics of rip channels on embayed beaches

Bruno Castelle [a,*], Giovanni Coco [b]

[a] CNRS, UMR EPOC, Université Bordeaux 1, France
[b] Environmental Hydraulics Institute, IH Cantabria, Universidad de Cantabria, Spain

ARTICLE INFO

Article history:
Received 7 November 2011
Received in revised form
13 April 2012
Accepted 16 April 2012
Available online 17 May 2012

Keywords:
Numerical modelling
Rip current
Morphodynamics
Embayed beach
Self-organization
Headland rip

ABSTRACT

We use a nonlinear morphodynamic model to examine the formation and nonlinear evolution of surfzone rip channels on embayed beaches. Starting from a range of embayed beach bathymetries characterized by different length and curvature, and under different time-invariant and time-varying wave conditions, the numerical model can reproduce the flow circulation and morphological characteristics observed on natural embayed beaches: (1) normal beach circulation, characterized by rips similar to non-embayed beaches and the presence of headland rips, (2) cellular circulation, with either headland rips only occurring at one or both ends of the embayment or a single rip at the centre of the beach and (3) transitional circulation, where both topography and currents influence rip location and behaviour. Time-invariant simulations show that, under oblique-wave forcing, rip spacing is systematically larger updrift than downdrift. Headland rips are preferably observed for straight beaches, with no clear dependence on wave angle. Wave shadowing and resulting alongshore gradients in wave height against the headland are the primary driving mechanism for headland rips. The formation of a single central rip is observed for short, curved embayed beaches, with no clear dependence on the wave angle as well. We use a novel non-dimensional embayment scaling parameter to quantify the degree of headland impact on beach circulation. Our simulations with shore-normal waves and initially alongshore-uniform embayed beaches show the parameter is consistent with observations. Our simulations also suggest that for high wave obliquity or time-varying wave angle to the shore, the influence of the headlands can progressively propagate into the whole domain. A time-varying wave angle results in persistent migration of rips towards the downcurrent headland rip, the splitting of shoals, an increase in merging of rip channels and more alongshore-variable rip spacing. The longshore variability of rip channel wavelength along embayed beaches is consistent with the hypothesis that rips are self-organized patterns and is consistent with recent field observations.

1. Introduction

Embayed sandy beaches are ubiquitous along hilly or mountainous wave-exposed coasts (e.g., Short and Masselink, 1999; Klein et al., 2010; Scott et al., 2011). The geometry of embayed beaches (headland and beach length) depends on the inherited geology or the presence of coastal structures which can deeply affect hydro- and morphodynamic processes. Embayed beaches are common worldwide and have inspired a large number of studies at different temporal scales. A number of models have been developed (e.g., Silvester, 1960; Hsu et al., 1989) to address the long-term behaviour (order of years) of the shoreline shape as a function of the local wave climate and the embayment geometry. At the intermediate scale (order of months) embayed beaches are often characterized by beach rotation (amongst many others, see for example Schyuer-Ming and Komar, 1994) with the alongshore direction of sand movement being associated with the dominant wave direction. Recently, Harley et al. (2011) showed that, at the intermediate scale, the beach rotation signal at Collaroy-Narrabeen Beach (Australia) is dominated by sediment exchange in the cross-shore rather than the alongshore direction, thus suggesting a more subtle conceptual model of beach rotation. Beach rotation is usually seasonal but periodic shifts related to wave climate have also been reported (Komar et al., 2000; Ranasinghe et al., 2004). Beach rotation can also occur as a fast response to individual storms possibly coupled to human activities (e.g., Ojeda and Guillen, 2008). Overall, at short time scales (order of days to weeks) embayed beaches are dynamic environments characterized by a variety of processes and a range of complex behaviours resulting in the presence of morphological patterns and the formation of rips (e.g., Holman et al., 2006; Gallop et al., 2011; Ojeda et al., 2011). The shorter time scale is the scale addressed in this study and is of particular relevance because rips are one of the most lethal hazards in the nearshore and are affected by the presence of headlands.

A study of 25 mostly embayed beaches along the Irish coast indicated the importance of the geological setting on morphological development and beach states (Jackson et al., 2005). In essence, as the geological factors regulate the source of beach material and the

* Corresponding author. Tel.: +33 05 40 00 29 65.
E-mail address: b.castelle@epoc.u-bordeaux1.fr (B. Castelle).

0278-4343/$ - see front matter © 2012 Elsevier Ltd. All rights reserved.
http://dx.doi.org/10.1016/j.csr.2012.04.010

volume of the accommodation space, the range of beach response to changes in wave climate can be limited compared to beaches in open coasts (Jackson et al., 2005; McNinch, 2004). Similarly, Short (2006) assessed the role of waves, sediment and tidal range in contributing to beach type for all the Australian beach systems. In some cases, Short (2006) indicated that geological inheritance was a major factor in defining beach type. Because of the variability in the degree of "control" posed by the geological setting, Short and Masselink (1999) synthesized the typical embayed beach hydrodynamic circulations into two main modes at different ends of the spectra and a third type that encompasses intermediate situations. More specifically: (1) normal beach circulation, where "normal" refers both to the presence of headland rips and the fact that the beach tends to behave as an open coast and therefore can be characterized by a large number of rips; (2) cellular circulation which stands at the opposite end of the spectra and is characterized by the dominance of the geological setting with rips only occurring at either the centre of the embayment or at one or both ends of the embayment; (3) transitional circulation which is an intermediate configuration with headland rip(s) and an increasing influence of the embayment size and shape on the surf zone circulation. In Short and Masselink (1999), there is no clear threshold to distinguish between normal and transitional circulations using observations. In this contribution, if the number of rips along the embayment (excluding headland rips) is larger than or equal to 4, we classify the circulation as "normal" (this is in qualitative agreement with the parameter proposed by Short and Masselink, 1999). Different types of embayed beach circulations are illustrated in Fig. 1.

Short and Masselink (1999) additionally used a non-dimensional embayment scaling parameter to quantify the degree of headland impact on beach circulation. The parameter they proposed depends on wave height and headland characteristics. Yet, in their approach they assumed that wave energy is redistributed along the whole wet–dry contour of the embayment. This implies that on embayed beaches where the headland length is larger than the surfzone width, the headland impact will be systematically overestimated. Another limitation is that the amount of wave energy dissipated against the headland is in most cases small compared to that dissipated along the beach. Accordingly, the non-dimensional embayment scaling parameter designed by Short and Masselink (1999) is misleading when addressing beach circulation for low- to moderate-energy wave conditions for embayed beaches with pronounced headlands. In order to quantify the degree of headland impact on beach circulation, we define a non-dimensional scaling parameter that considers the number, δ, of surf zone widths, X_s, that fit into an embayment of length L. If we consider a beach with a surf zone slope β exposed to

Fig. 1. Examples of typical embayed beach circulations as described in Short and Masselink (1999). (a) Cellular beach circulation with a rip current at the centre of the beach at Tamarama Beach in Sydney (New South Wales, Australia). Rip location is highlighted by the presence of dye (courtesy of R.W. Brander). (b) Cellular beach circulation with one headland rip at the same beach (courtesy of R.W. Brander). (c) Cellular circulation at St. James Point (South Australia). The two headland rips can be deduced from (headland in the upper part of the image) the dark area in the breaker and (headland in the lower part of the image) the sediment plume (source: Google Earth). (d) Transitional beach circulation at Bondi Beach (New South Wales, Australia) with one headland rip and additional rip channels away from the headland. (e) Transitional beach circulation at Blueys Beach (New South Wales, Australia) with one headland rip and two additional rip channels within the embayment (courtesy of A.D. Short). (f) Normal beach circulation at Seal Rocks (New South Wales, Australia) with one headland rip and six to seven additional rip channels along the beach (courtesy of A.D. Short).

waves with a significant wave height H_s, then we can assume $X_s = H_s/(\gamma_b \beta)$ where γ_b is the breaking parameter (here equal to 0.73; Battjes and Stive, 1985). Accordingly, the non-dimensional embayment scaling parameter reads:

$$\delta = \frac{L\gamma_b \beta}{H_s} \quad (1)$$

Studies linking the high-frequency response of rips on embayed beaches to changes in tidal and wave conditions are scarce. Holman et al. (2006) studied surfzone sandbar dynamics on an embayed, single-barred, beach with reasonably large length compared to the offshore extent of the headlands. The study site was located in the central part of the embayment. Thus, rips were likely not directly influenced by the headlands. Gallop et al. (2011) studied an embayed beach characterized by shorter length (especially when compared to the offshore extent of the headlands) and noted the persistent occurrence of headland rips and an evident longshore variability in the spacing between rip channels. On a beach where the ratio between the headland protrusion and the beach length is even larger, Enjalbert et al. (2011) observed the expected headland rips and the common formation of a transient rip channel developing at a fixed location along the embayment. This rip channel subsequently migrates to merge with rips further along the beach. Enjalbert et al. (2011) also noted that, during severe storms, sandbar three-dimensionality rapidly increases which is in contrast with observations on open beaches that are typically characterized by a system reset (i.e., decrease in beach three-dimensionality as a result of an up-state sequence e.g., Wright and Short, 1984; Van Enckevort et al., 2004) and that develop sandbar three-dimensionality only if sustained large waves are present (Van Enckevort et al., 2004; Splinter et al., 2011). Table 1 synthesizes these studies and other existing documented embayed beach sites at which sufficient material is provided to indicate the observed beach circulation and to compute the embayment parameter δ.

Similar to the relatively small number of field observations, only a limited number of numerical studies describe embayed beaches. Rip current development on a semi-elliptical beach has been studied by Silva et al. (2010) and results indicated, for the specific geometry analysed, the presence of cellular circulation characterized by a central rip. In terms of morphodynamics, Yamashita and Tsuchiya (1992) used a numerical model to simulate pocket beach formation and focussed on the evolution of the shoreline position. They found no evident circulation cells except close to the headland. Daly et al. (2011) used the same type of process-based model to investigate beach rotation for one embayed beach configuration and 16 different wave conditions. The authors used a non-barred beach, therefore limiting the range of dynamics related to rip channels. Simulations resulted in the formation of a stable bay shape that was highly dependent on the incident wave conditions. Ribas et al. (2007) applied a nonlinear morphodynamic model to the artificial embayed beaches of Barcelona (Spain). The model was able to simulate two events of crescentic bar formation. Yet, periodic lateral boundary conditions without headland were considered, therefore preventing the investigation of the impact of the embayment on 3D sandbar evolution. Finally, Reniers et al. (2004) studied the effect of wave-groups on the development of rip channels on an embayed beach. The primary objective of their study was to assess the effects of wave group forcing on the surfzone sandbar response, and the impact of the beach geometry was not studied systematically. Addressing the phase resolution of the mean and infragravity motions on a fixed alongshore-uniform bathymetry, Reniers et al. (2004) showed that including directional spreading in the initial wave conditions affects the behaviour of rip channels. They noted no clear evidence of a dominant standing edge wave mode but they further observed an increased contribution of trapped edge waves to the total infragravity motions concurrent with rip channel development. Reniers et al. (2004) concluded that infragravity waves are not required to generate the quasi-periodic rip channels (or crescentic bars) on an embayed beach, and that the observed preference in length scale for the edge wave motions is the result of the underlying bathymetry and not the other way around. This confirms that, on embayed beaches as well as for open beaches, three-dimensional (3D) surfzone sandbar patterns such as rip channels and crescentic bedforms can develop through the positive feedback between flow, sediment transport and the evolving bathymetries (e.g., Deigaard et al., 1999; Falqués et al., 2000; Calvete et al., 2005; Smit et al., 2008; Castelle and Ruessink, 2011) and that the presence of standing edge waves is not a necessary requirement (Coco and Murray, 2007).

Overall, the influence of the embayment geometry (length and shape of the beach, cross-shore extent of the headlands) on the formation and subsequent evolution of surfzone rip channels has never been studied using a nonlinear morphodynamic model. In this paper we address this problem which, aside from its scientific interest, is critical to predict the characteristics of one of the most deadly coastal hazards (e.g., MacMahan et al., 2006; Scott et al., 2007) and a key element of mixing in nearshore hydrodynamics (Dalrymple et al., 2011). A nonlinear morphodynamic model (Section 2) is used herein to simulate the development of surfzone rip channels on a number of embayed beach geometries. Results (Section 3) are discussed in Section 4 in the framework of existing observations of rip channels on embayed beaches.

2. Methodology

2.1. Numerical model

A nonlinear morphodynamic model (detailed in Castelle and Ruessink, 2011; Castelle et al., 2012) is used to simulate the formation, subsequent nonlinear evolution of the rip channels and associated shoreline rhythmic features (megacusps) as well as the saturation of the bedform growth. The model describes nearshore hydrodynamics coupling the spectral wave model SWAN (Booij et al., 1999) and a short-wave averaged and depth-integrated flow model. Hydrodynamics in turn drive a model addressing sediment transport and bottom changes. This approach has already been successfully used to study rip current dynamics (e.g., Castelle and Bonneton, 2006) and 3D

Table 1
Observations of embayed beach circulation ordered by publication year. Wave data correspond to prevailing wave conditions, except in Loureiro et al. (2012) which corresponds to a single storm event resulting in the formation of mega-rips.

	L (m)	β	Hs (m)	δ	Type of rips	Reference
Engine head bay (Jamaica)	350	0.028	0.5	14.3	Transitional; Headland rips and central rip	Huntley et al. (1988)
Palm Beach (Australia)	2000	0.02	1.5	19.5	Normal; No headland rip	Holman et al. (2006)
La Barceloneta (Spain)	1100	0.033	1.1	24.1	Normal; Headland rips	Ribas et al. (2007)
Tairua (New Zealand)	1200	0.03	0.56	46.9	Normal; Headland rips	Gallop et al., 2011
Biarritz (France)	1200	0.02	1.57	11.2	Transitional; Headland rips	Enjalbert et al. (2011)
Arrifana (Portugal)	1340	0.038	5.5	6.8	Cellular; Headland rips	Loureiro et al. (2012)

surfzone sandbar morphodynamics (e.g., Castelle et al., 2010). In this study, the shape of the offshore wave spectrum is the default JONSWAP with a narrow directional spreading of 8° while diffraction is not accounted for. The effect of directional spreading and wave diffraction will be discussed later in the paper.

In the flow model, the nonlinear shallow water equations comprise the continuity equation:

$$\frac{\partial \eta}{\partial t}+\frac{\partial Q_i}{\partial x_i}=0 \tag{2}$$

where t is time; η is the mean free surface elevation; $Q_i=hU_i$ is the water volume fluxes with the subscript $_i$ referring to the two horizontal coordinates (x and y represent the alongshore and cross-shore axis, respectively); U_i is the wave-driven mass-flux velocity according to Mei (1989); h is the mean water depth. The momentum balance equation is defined as:

$$\frac{\partial Q_i}{\partial t}+\frac{\partial}{\partial x_j}\left(\frac{Q_iQ_j}{h}\right)+gh\frac{\partial \eta}{\partial x_i}+\frac{1}{\rho}\frac{\partial S_{ij}}{\partial x_j}-\frac{1}{\rho}\frac{\partial T_{ij}}{\partial x_j}+\frac{\tau_i^b}{\rho}=0 \tag{3}$$

where g is the gravitational acceleration; ρ is the water density; S_{ij} is the radiation stress tensor (Philipps, 1977); $\tau_i^b=\rho C_f u_{rms}U_i$ is the bed shear stress; u_{rms} is the root mean square wave orbital velocity at the bottom; C_f is a bottom friction coefficient (equal to 0.0045 in the present study) and T_{ij} is the lateral mixing term which describes the horizontal momentum exchange due to the combined action of turbulence and mean current using the formulation proposed by Battjes (1975):

$$T_{ij}=\rho h\nu\left(\frac{\partial U_i}{\partial x_j}+\frac{\partial U_j}{\partial x_i}\right) \tag{4}$$

where the eddy viscosity ν is defined as:

$$\nu=Mh\left(\frac{D}{\rho}\right)^{1/3}+\nu_0 \tag{5}$$

where D is the rate of energy loss through depth-induced wave breaking; M is a dimensionless coefficient (taken as 2 in the present study) and ν_0 is a constant eddy viscosity (taken as 2 $m^2\,s^{-1}$ in the present study). The slightly larger eddy viscosity is used to damp, potentially, purely hydrodynamic instabilities in the wave set-up and flow circulation.

The sediment transport $\vec{Q}_s$ is computed as:

$$\vec{Q}_s=\alpha(\overline{\overline{|\vec{u}_b(t)|^3\vec{u}_b(t)}}-\gamma u_{rms}\vec{\nabla}Z) \tag{6}$$

where α is a stirring factor set to 2×10^{-4} $s^3\,m^{-2}$; γ is a bedslope coefficient (equal to 100 $m^3\,s^{-3}$ in the present study); $\vec{\nabla}$ is the horizontal gradient operator and $\vec{u}_b(t)=\vec{U}+(u_{rms}\cos\omega t)\vec{e}_k$ is the total flow velocity at the seabed (mean currents and orbital velocity) assuming linear waves with ω being the wave angular frequency and $\vec{e}_k$ the unit vector along the wave ray, both based on spectral peak. The $\overline{\overline{()}}$ notation defines time-averaging over a duration longer than the typical wave period. Z is the bed level deviation from initial equilibrium calculated as $Z=Z_f-Z_f^0$ where Z_f and Z_f^0 are the seabed level and the initial equilibrium beach profile, i.e. the bed level at the basic state. Consistent with a widely accepted approach (e.g., Garnier et al., 2006, 2008; Castelle and Ruessink, 2011), we assume the presence of a basic state meaning that the cross-shore transport driven by wave nonlinearities and undertow is in balance with the gravitational downslope transport for a given equilibrium cross-shore beach profile Z_f^0. Because the advective part in our sediment transport formula (6), similar to the suspended sediment load in Bailard (1981), is different from that in Garnier et al. (2006, 2008) our reference values of α and γ are not directly comparable. Yet, simulated rip channel systems and wave-driven circulations are similar in patterns and grow over similar timescales.

The new seabed level Z_f was computed using the sediment mass conservation equation:

$$\frac{\partial Z_f}{\partial t}+\frac{1}{1-p}\vec{\nabla}\vec{Q}_s=0 \tag{7}$$

where $p=0.4$ is the sediment porosity. The morphological time step for the bed update scheme, which is different from the hydrodynamic time step (1 s), was 1 h for all the simulations presented herein.

We used periodic lateral boundary conditions and a 0-mass flux boundary condition across the headland. We therefore assumed an infinite number of embayed beaches of similar size and shape. This implies that, ultimately, headland sediment bypassing can occur for long-term simulations with large wave angles (when beach rotation becomes significant). SWAN simulations were run over a bathymetry generated by a sequence of three embayed beaches (the three beaches are exactly the same). Driving forces were extracted at the central embayment to prevent potential edge effects for waves with both high obliquity and large directional spreading.

2.2. Model set-up

Two main configurations were used to apply the model to different initial embayed bathymetries: rectilinear (Fig. 2a) or curved shape (Fig. 2b). The headland length was kept constant (450 m) and the alongshore length was varied (L=500, 1000, 2000, 4000 and 8000 m). A 40-m seaward shoreline extent at the headland was applied to the curved configuration (Fig. 2b). To address the effect of headlands on rip channel morphodynamics, additional simulations on a 8000-m long alongshore-uniform

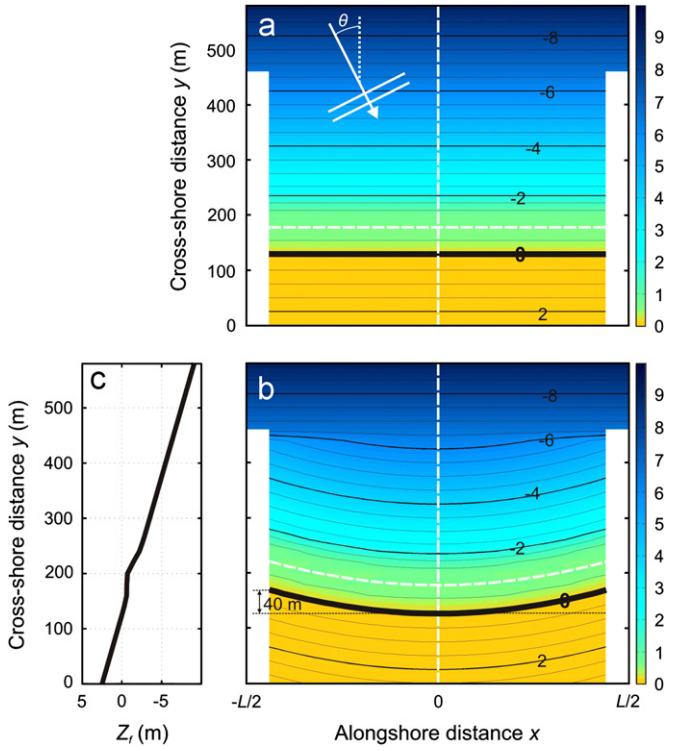

Fig. 2. (a) Initial (basic state) alongshore-uniform embayed beach exposed to waves with an angle of incidence θ. (b) Initial (basic state) curved embayed beach bathymetry. (c) Single-barred beach profile used to build the initial embayed beach bathymetries. The alongshore dotted white line in a and b indicates the location of the alongshore beach profile Z_b used in the analysis, L is the alongshore length of the domain, the thick black line indicates the 0-m sea level shoreline, colour bars show seabed elevation in meters and the cross-shore white dotted line indicates the location of the beach profile in (c).

open beach (no headland) were performed. To avoid the complicated feedbacks governing multi-barred beach dynamics (e.g., Ruessink et al., 2007; Castelle et al., 2010), only the behaviour of single-barred embayed beaches was investigated here. The basic state consisted of a beach with a 1:50 planar sloping depth profile. A sandbar, located 90 m from the mean-sea-level shoreline with its crest in 0.8 m water depth, was superimposed on the planar profile (Fig. 2c). The computational grid had an alongshore and a cross-shore length of L and 580 m, respectively, with 20×20 m grid cells. Random perturbations with a magnitude of 1 mm in the seabed were superimposed on the initial beach bathymetries to excite nearshore feedbacks and the growth of morphological perturbations.

For each initial bathymetry, time-invariant wave forcing is applied at the offshore boundary with a significant wave height $H_s=1$ m, a peak wave period $T_p=10$ s and a wave angle perpendicular to the shore $\theta=0^\circ$, 5° and 10° (anticlockwise is positive for the frame of reference adopted). Additional simulations were done for time-varying wave angle (we used a sine wave shape with a 0-mean θ, amplitude $A=5^\circ$ or 10° and a period $T=4$ days, see Castelle and Ruessink, 2011, for further details). Accordingly, the different alongshore lengths of the embayed beach ($L=500$, 1000, 2000, 4000 and 8000 m) correspond to an embayment scaling parameter $\delta=7.3$, 14.6, 29.2, 58.4 and 116.8. Overall, a total of 50 embayed-beach simulations, each characterized by a 60-day duration, i.e. 1440 morphological time steps, have been performed and analysed. To examine the evolution of rip channels, the alongshore profile at $y=180$ m between the bar crest and the mean-sea-level shoreline denoted $Z_b(x,t)$ (Fig. 2a) was computed at every time step. A curved alongshore profile (Fig. 2b) was applied at the same location for the curved bathymetries. Tests have confirmed this location is representative of the overall rip channel evolution. We additionally counted the number of rip channels (comprising the headland rips) along the beach N_{rip} to estimate the mean rip spacing λ defined as N_{rip}/L. For short embayed beaches (with only one to three rips comprising the headland rips), the term "mean" is inadequate and is only used for consistency with the other simulations.

3. Results

We first briefly describe rip channel morphodynamics along open beaches. Then, we analyse in detail a typical simulation of rip channel formation and evolution on an embayed beach. Finally, we examine rip channel morphodynamics on embayed beaches for time-invariant and time-varying wave forcing, respectively.

3.1. Open beach (no headland) simulations

Fig. 3 shows the time evolution of the alongshore profile Z_b on an open beach for time-invariant forcing with $H_s=1$ m, $T_p=10$ s and $\theta=0^\circ$, 5° and 10°, with a zoom at 2000 m $< x <$ 4000 m of the rip channel morphology and superimposed wave-driven circulation at $t=10$ days. The model shows that for $\theta=0^\circ$, 5° and 10°, rip channels stabilize at a narrow range of wavelengths with a mean λ of about 320, 440 and 600 m, respectively (Fig. 3a–c). A notable difference with Castelle and Ruessink (2011) and Castelle et al. (2012) is the smaller, more realistic, rip spacings obtained as a result of the slight changes in hydrodynamic parameters (M, v_0 and C_f). Rip channel migration rate and beach three-dimensionality increase and decrease with increasing θ, respectively. These results are in line with existing linear or nonlinear stability analyses for open coasts (e.g., Calvete et al., 2005; Garnier et al., 2008). In addition, our model shows that megacusps are more pronounced for shore-normal waves. For $\theta=0$ and 5°, clear shore-normal and skewed rip current circulations are observed, respectively (Fig. 3d and e). In contrast, a meandering longshore current is observed for $\theta=10^\circ$ (Fig. 3f).

3.2. Example of typical rip channel morphodynamics on an embayed beach

Fig. 4 shows the time evolution of rip channels on a curved embayed beach with $L=2000$ m ($\delta=29.2$), for time-invariant forcing with $H_s=1$ m, $T_p=10$ s and $\theta=5^\circ$. Results show that at $t=0$ (Fig. 4a) the longshore current dominates the circulation within the entire embayment. As expected, the longshore current is larger in the updrift (left) part of the beach (≈ 0.55 m s^{-1}) than in the downdrift (right) part (≈ 0.15 m s^{-1}) because of beach curvature. One rip current is observed against each headland. The updrift headland rip is larger (≈ 0.4 m s^{-1}) than the downdrift one (≈ 0.1 m s^{-1}). At $t=5$ days (Fig. 4b), a rip channel formed against each headland. Three additional rip channels are observed within the embayment at $x \approx 0$, 400 and 650 m. The downdrift headland rip is more intense (≈ 0.65 m s^{-1}) than the updrift one (≈ 0.5 m s^{-1}), which is in the same order of magnitude of the three other rips within the embayment (Fig. 4b). A strong longshore current ($\approx 0.6-0.7$ m s^{-1}) dominates the updrift part of the embayment. The same applies at $t=10$ days (Fig. 4c) with the notable exception that the rip channel located at $x=400$ m at $t=5$ days merged to the rip channel at $x=650$ m. Also, the rip that initially appeared at $x=0$ m has further developed and migrated to $x=150$ m. Overall, for the simulation shown in Fig. 4, the resulting beach circulation pattern at $t=10$ days can be referred to as transitional in the Short and Masselink (1999) classification with two headland rips and two additional rips within the embayment.

The corresponding time evolution of the alongshore profile Z_b given in Fig. 4d shows at $t \approx 9$ days the merging of the two rip channels into a rip channel at $x=600$ m that subsequently merges to the downdrift headland rip channel at $t \approx 35$ days. The other rip channel remains quasi stationary for $t > 35$ days. For $t > 25$ days, transient rip channels persistently form, migrate downdrift and subsequently merge to the rip channel further downdrift (Fig. 4d).

Over the course of the simulation, beach rotation increases. Simulations with $\theta=10^\circ$ showed that for larger wave obliquity beach rotation can become a dominant factor by the end of the 60-day simulation. The basic state approach in the model (for more details see Castelle and Ruessink, 2011) is not consistent with a rotated beach and can ultimately result in unrealistic morphodynamic behaviour. Beach rotation will be discussed later in the paper and in the following we focus on the first 20 days of the simulations.

3.3. Time-invariant simulations

Fig. 5 shows the time evolution of the alongshore profile Z_b for time-invariant wave forcing with $H_s=1$ m, $T_p=10$ s and $\theta=0^\circ$ (left-hand panels), 5° (middle panels) and 10° (right-hand panels). Simulations are shown for alongshore-uniform (top panels) and curved (bottom panels) embayed beaches for $L=500$, 1000, 2000 and 4000 m. Simulations with $L=8000$ m are not shown as they are essentially the same as the ones with $L=4000$ m with the exception that more rip channels are observed within the embayment.

Results show that, for alongshore-uniform embayed beaches under shore-normal waves (Fig. 5a, d, g and j), headland rip channels are systematically observed. The impact of the headland on rip spacing λ is important only for short beaches. For $L=500$ m (Fig. 5a), rip channel formation within the embayment is inhibited; for $L=1000$ m (Fig. 5d) one rip forms at the centre of the

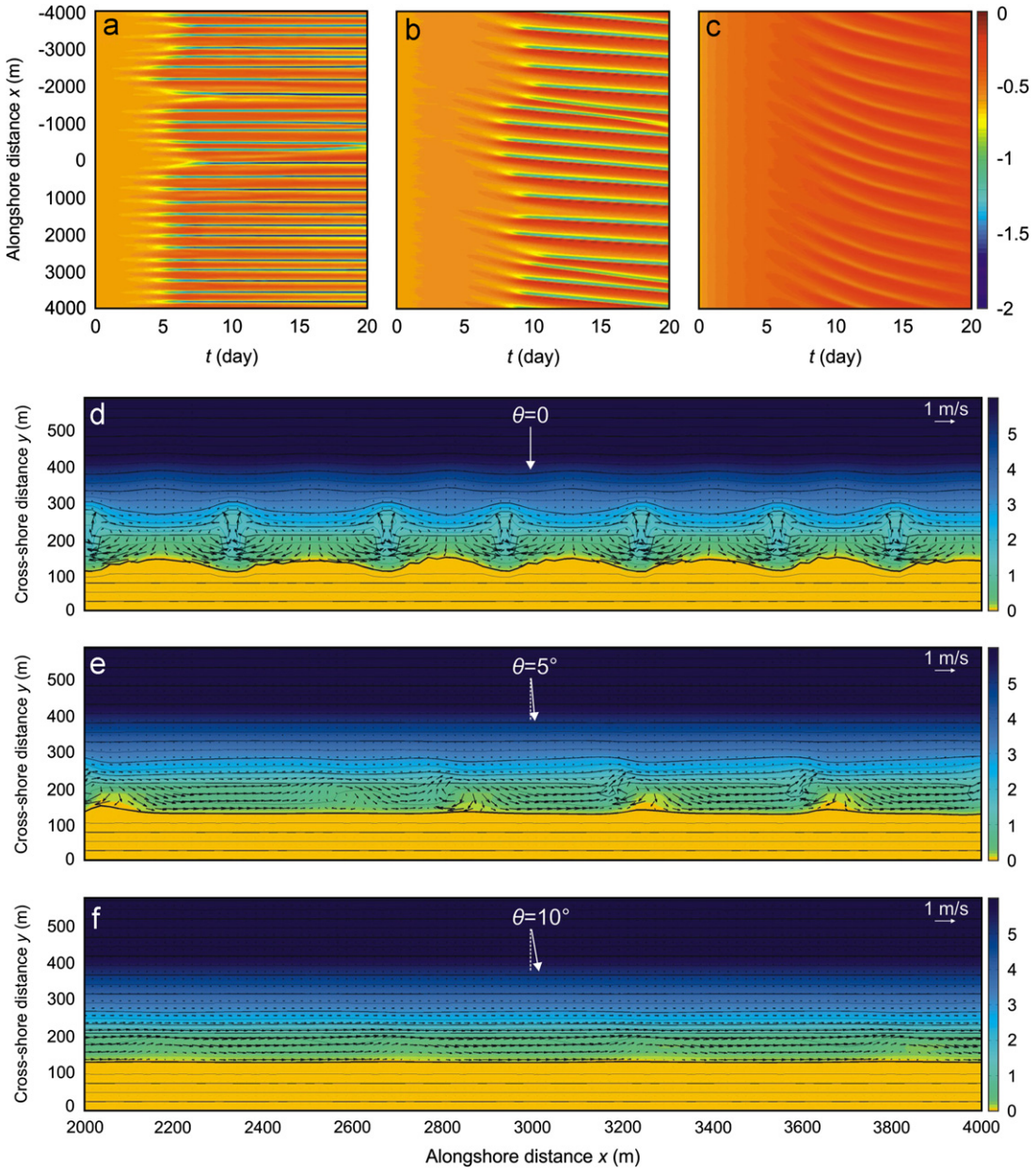

Fig. 3. Evolution of surfzone rip channels starting from an alongshore-uniform open beach (no headland) for time-invariant wave forcing with $H_s=1$ m, $T_p=10$ s and (a,d) $\theta=0^\circ$, (b,e) $\theta=5^\circ$, (c,f) $\theta=10^\circ$. Top panels show the time evolution of the alongshore profile Z_b, and bottom panels show a zoom at 2000 m $< x <$ 4000 m of the beach morphology with superimposed wave-driven circulation at $t=10$ days. In all panels colour bar indicates seabed elevation in meters.

beach ($\lambda=500$ m); for $L=2000$ m (Fig. 5g) and $L=4000$ m (Fig. 5j), a total N_{rip} of 6 and 12 rip channels are observed ($\lambda=333$ m). The latter case is characterized by a similar rip spacing as for the open beach case (Fig. 3) and so falls in the category of normal beach circulation (Short and Masselink, 1999).

Results for alongshore-uniform beaches (Fig. 5a–l) also show that the impact of wave obliquity on rip channel behaviour is large, with the exception of headland rips which are systematically present. As for linear and nonlinear modelling studies of rip channel behaviour on open beaches (e.g., Deigaard et al., 1999; Calvete et al., 2005; Garnier et al., 2008; Castelle and Ruessink, 2011, see also Fig. 3) both rip spacing and rip migration increase with increasing θ. Rip channels often merge with the downdrift headland rip (e.g., Fig. 5k at $t=15$ days). Under oblique waves the impact of headlands on rip spacing is stronger than for shore-normal waves. For instance, for $L=4000$ m and $\theta=5^\circ$ (Fig. 5k) $N_{rip}=7$, corresponding to a mean rip spacing $\lambda\approx570$ m, which is substantially larger than the mean rip spacing of 440 m found in the open-beach (no headlands) scenario (Fig. 3b). In addition, simulations with oblique waves almost systematically result in alongshore variable rip spacing.

Similar results were obtained for curved embayed beaches (Fig. 5m–x) with a few noteworthy exceptions. Rip channels against the two headlands are not systematically observed (e.g., Fig. 5m, n, p). For instance, the simulation starting from a curved embayed beach with $L=500$ m and $\theta=0^\circ$ or 5° results in a cellular beach circulation with one rip channel at the centre of the beach and no headland rip (Fig. 5m and n), which contrasts with the headland rips situations for alongshore-uniform embayed beaches. This different behaviour is illustrated in Fig. 6 that details the hydrodynamics at $t=0$ for the alongshore-uniform and the curved embayed beach. For the alongshore-uniform

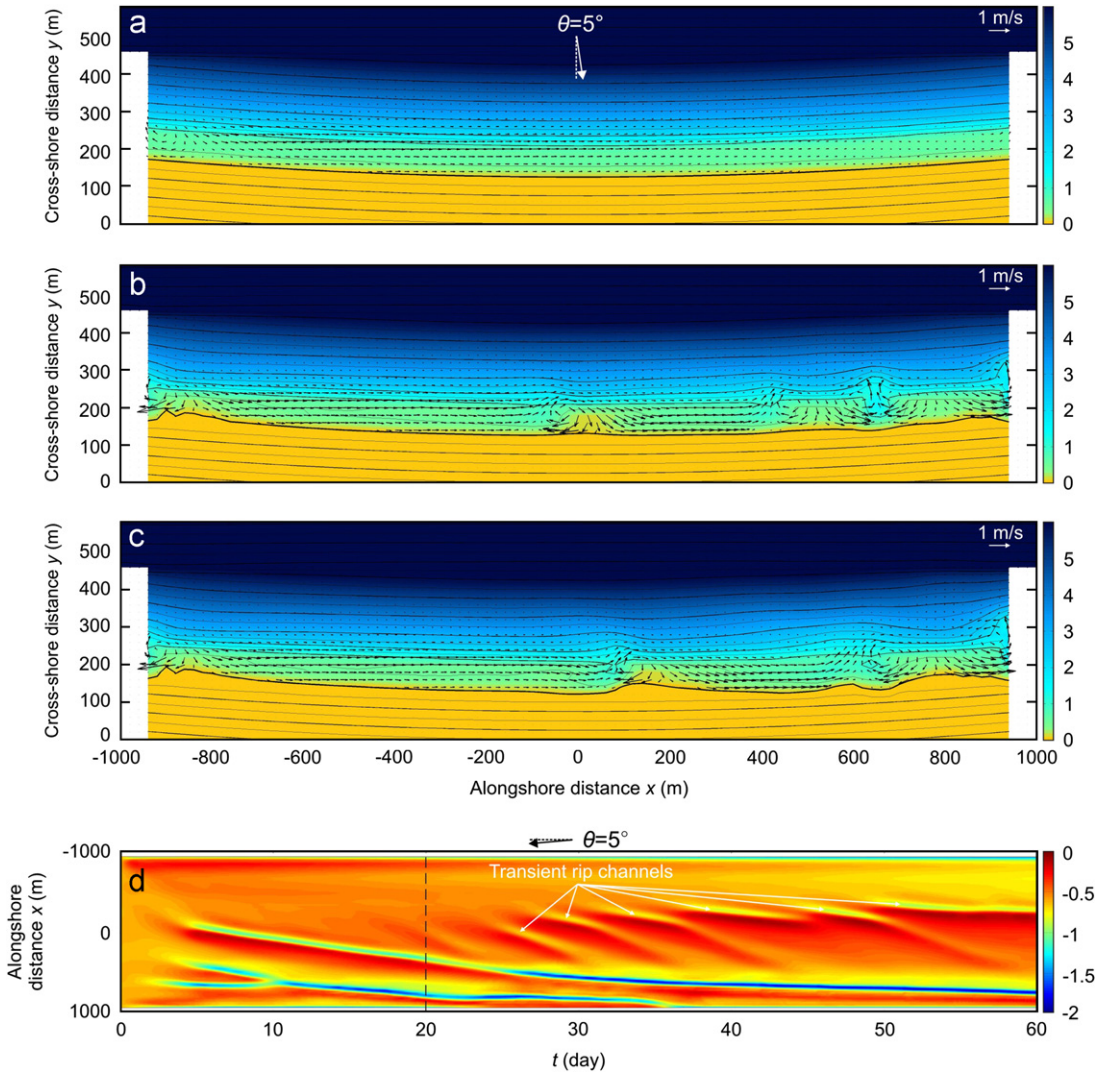

Fig. 4. Evolution of surfzone rip channels with superimposed wave-driven circulations for $H_s=1$ m, $T_p=10$ s and $\theta=5^\circ$, starting from a curved embayed beach with $L=1000$ m. (a) $t=0$, (b) $t=5$ days, (c) $t=10$ days. (d) Resulting time evolution of the alongshore profile Z_b with the vertical dashed line indicating $t=20$ days at which beach rotation is still negligible for all simulations.

embayed beach (left-hand panels), the increasing wave heights at the centre of the beach (Fig. 6a) due to wave shadowing lead to a slightly larger amplitude of set-up and set-down in the surf and shoaling zone, respectively (Fig. 6b). The vectorial sum of the resulting gradients in radiation stress $\overrightarrow{F_w}$ ($F_{wi}=-(1/\rho)\partial S_{ij}/\partial x_j$, Fig. 6a) and pressure gradients $\overrightarrow{F_p}$ ($F_{pi}=-gh\partial\eta/\partial x_i$, Fig. 6b) gives the residual forcing $\overrightarrow{F_r}$ (Fig. 6c). $\overrightarrow{F_r}$, which, for open beaches, is essentially similar to the vorticity forcing term derived from the differential broken wave energy dissipation (Bonneton et al., 2010; Bruneau et al., 2011), indicates how much net forcing is available to drive nearshore currents (Haas et al., 2002; Castelle and Bonneton, 2006). This forcing therefore drives two headland rips (Fig. 6d). The resulting sediment transport patterns result in beach erosion against each headland and lead to the subsequent formation of two headland rip channels at $t=2$ days (Fig. 6e). This contrasts with the results starting from a curved embayed beach (right-hand panels in Fig. 6) for which wave energy focussing through wave refraction across the curved nearshore bathymetry overwhelms wave shadowing near the headlands. This results in slightly larger wave heights at the headlands (Fig. 6f) and slightly smaller amplitude of set-up and set-down in the surf and shoaling zone at the centre of the beach, respectively (Fig. 6g). In turn, there is a reversal in residual forcing (Fig. 6h) that drives a rip current near the centre of the beach (Fig. 6i) and the formation of a rip channel at $t=2$ days (Fig. 6j).

For a given offshore wave forcing and larger beach length L, the number of rip channels N_{rip} is generally the same or smaller for curved beaches than for alongshore-uniform embayed beaches. For shore-normal waves, rip spacing systematically increases with decreasing distance to the headland as rips tend to migrate toward the centre of the beach as a result of beach curvature (e.g., Fig. 5v).

3.4. Time-varying simulations

Fig. 7 shows the time evolution of the alongshore profile Z_b for $H_s=1$ m, $T_p=10$ s and time-varying angle of wave incidence with an amplitude $A=5^\circ$ and 10°. We started the numerical simulations considering an alongshore-uniform embayed beach with $L=500$, 1000, 2000, 4000 and 8000 m. Given that no beach rotation occurs (wave climate is characterized by 0-mean in θ), here we show the results for a 30-day duration simulation. Results show that rip channel evolution for $A=5^\circ$ (left-hand panels in Fig. 7) are similar to that with time-invariant shore-normal waves (Fig. 5a, d, g and j)

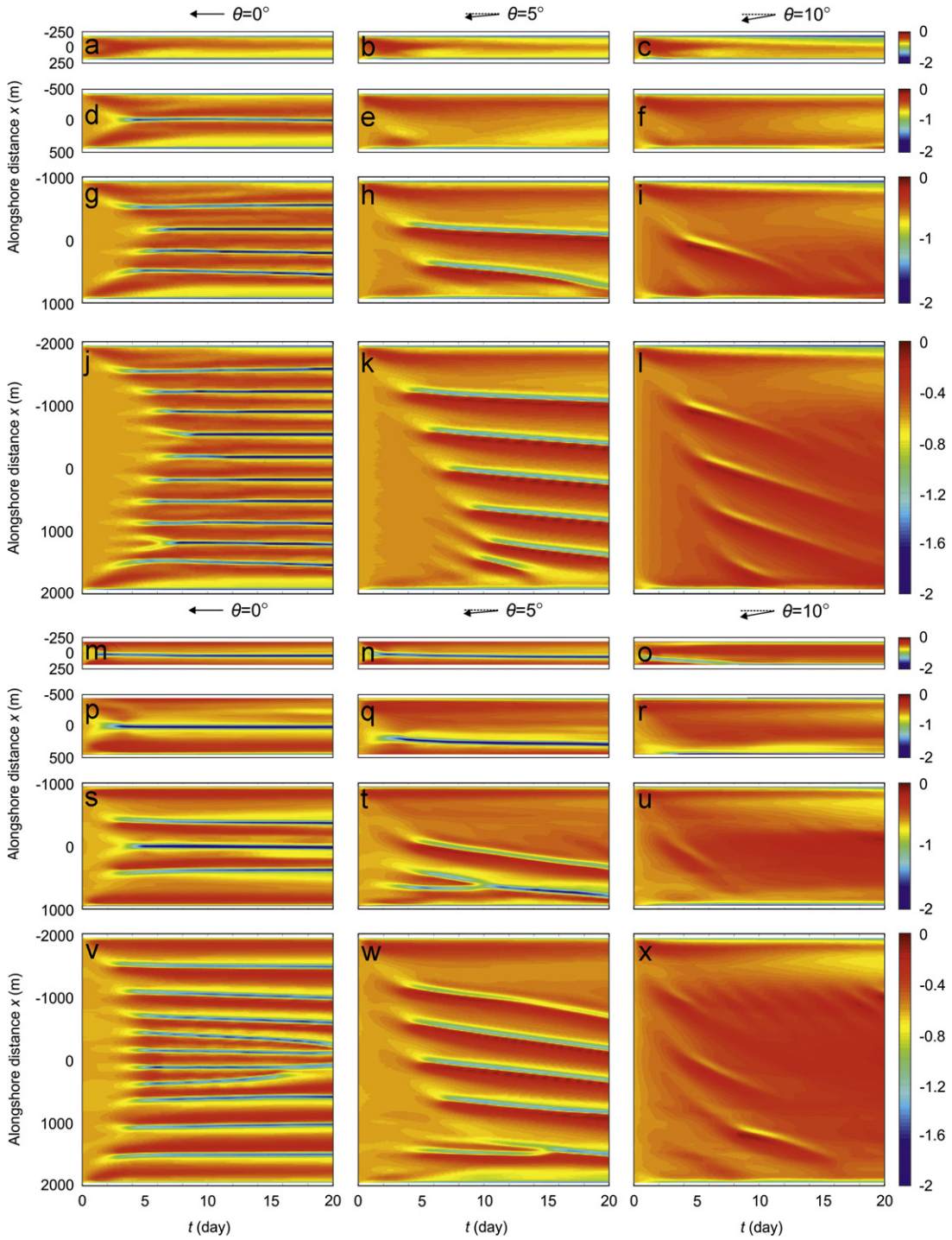

Fig. 5. (a–l) Time evolution of the alongshore profile Z_b starting from an alongshore-uniform embayed beach and for time-invariant wave conditions with $H_s=1$ m, $T_p=10$ s and (left-hand panels) $\theta=0^\circ$, (middle panels) $\theta=5^\circ$ and (right-hand panels) $\theta=10^\circ$. (a–c) $L=500$ m, (d–f) $L=1000$ m, (g–i) $L=2000$ m, (j–l) $L=4000$ m. (m–x) is the same starting from a curved embayed beach.

with few notable exceptions. For $L>1000$ m, time-invariant forcing results in the splitting of shoals (see Fig. 7i for examples of splitting of shoal). This is consistent with the recent modelling exercise of Castelle and Ruessink (2011) who showed that a time-varying wave angle of incidence results in the increase in merging and the splitting, that contrasts with the limited number of mergings and the absence of splitting for time-invariant forcing simulations (see also Fig. 3). This results in slightly different mean rip spacing than for the time-invariant shore-normal wave simulation.

For $A=10^\circ$, the impact of time-varying θ on rip channel morphodynamics is more profound. Rip channel evolution is the same as for the time-invariant forcing only for the case of $L=500$ m with two persistent headland rips. For larger L, splitting of shoals is ubiquitous. For instance, it results in the formation of two rip channels within the embayment for $L=1000$ m (Fig. 7d) instead of the single rip observed for the time-invariant simulation (Fig. 5d). In addition, for $L>1000$ m (Fig. 7f, h and j), rip channels that are located in the vicinity of the headland are systematically drawn towards the headland rip.

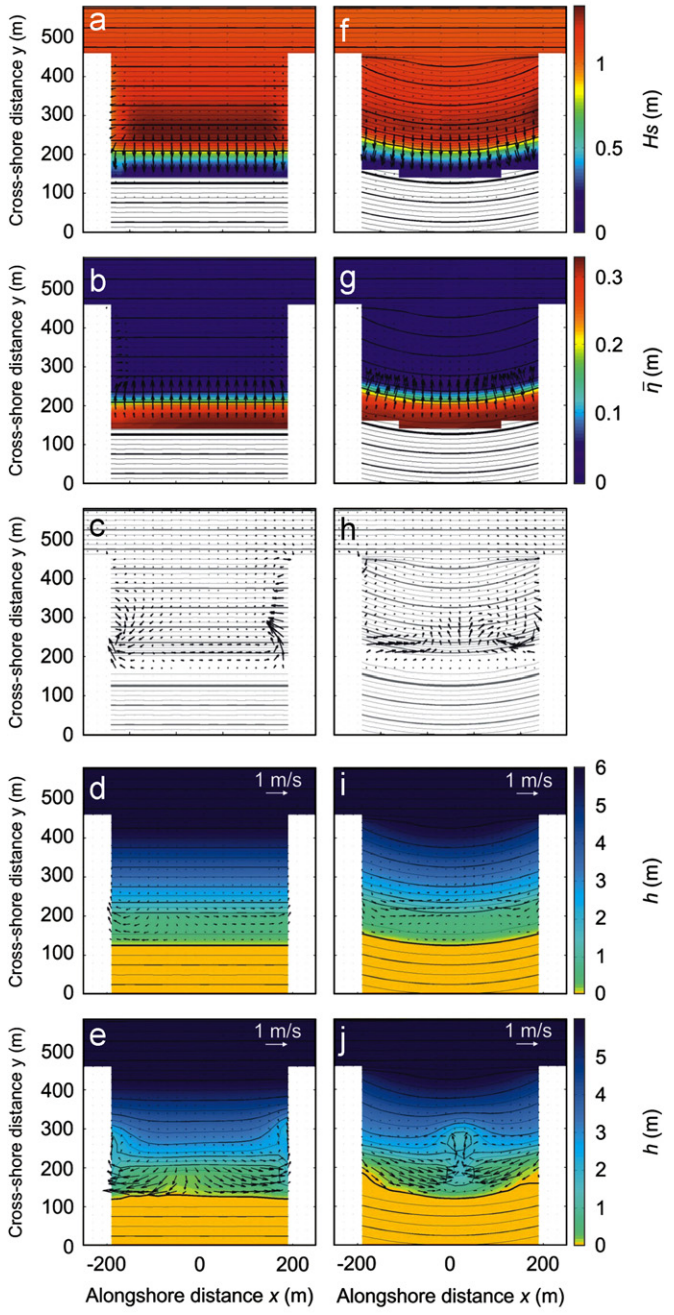

Fig. 6. Hydrodynamics at $t=0$ for offshore waves with $H_s=1$ m, $T_p=10$ s and $\theta=5^\circ$ starting from an embayed beach with $L=500$ m and an alongshore-uniform (left-hand panels) and a curved shape (right-hand panels). (a,f) Wave field with colour bar indicating significant wave height H_s in meters and resulting gradients in radiation stress $\overrightarrow{F_w}$ (arrows) with $F_{wi}=-(1/\rho)\partial S_{ij}/\partial x_j$. (b,g) Pressure gradients $\overrightarrow{F_p}$ (arrows) with $F_{pi}=-gh\partial\eta/\partial x_i$, superimposed on the η field with colour bar indicating η in meters. (c,h) Residual forcing $\overrightarrow{F_r}=\overrightarrow{F_p}+\overrightarrow{F_w}$ (arrows). (d,i) Resulting wave-driven circulation with colour bar indicating water depth in meters. (e,j) Evolution of wave-driven circulation and bottom evolution at $t=2$ days. In all panels is-contours (0.5-m intervals) are contoured in the background.

This feeds back onto the behaviour of the morphology at the larger spatial scale. The increase of rip spacing results in the splitting of the nearby shoals as rip channels continuously attempt to self-organize into a more alongshore-uniform spatial pattern (e.g., Fig. 5h). As a result, at times, the alongshore spacing is not regular and even the mean spacing changes throughout the simulation. For instance, for $L=2000$ m (Fig. 7f) three and five rip channels are observed within the embayment at $t\approx10$ and 25 days, respectively.

Overall, for $L\leq2000$ m, time-varying forcing is crucial to understand sources of variability in rip channel morphodynamics. In fact, simulations with time-varying forcing show drivers of change in mean rip spacing as well as an increase in the nonlinear behaviour of rip channels (i.e. merging and splitting). The simulations starting from curved embayed beaches showed similar results as those given in Fig. 7 except that rips in the vicinity of the headlands are less effective in "attracting" the nearby rips.

4. Discussion and conclusions

In this paper the nonlinear morphodynamic modelling of rip channels on embayed beaches was addressed. Starting from a number of idealized bathymetries and for different synthetic time-invariant and time-varying wave conditions, all the embayed beach circulation patterns deduced from field observations in Short and Masselink (1999) can be reproduced with the present numerical model. Fig. 8 shows some examples of embayed beach circulation patterns (all after 10 days of simulation). We found that cellular circulation with headland rips (Fig. 8a) is favoured by both small beach curvature and short beach length while cellular circulation with a rip at the centre (Fig. 8b) is favoured by large beach curvature and short beach length due to the residual forcing $\overrightarrow{F_r}$ (Fig. 6). Transitional circulation with an updrift headland rip and a rip further along the beach (Fig. 8c) is favoured by large values of wave obliquity and beach curvature, and by a reasonably small beach length. When increasing the beach length further, transitional rip circulation with headland rips and one to three additional rips along the beach is observed (e.g., Fig. 8d). Increasing the beach length even further (or decreasing the angle of wave approach and/or beach curvature) results in normal circulation with the development of four or more rips not affected by the headlands (even though headland rips are still present, Fig. 8e) whose spacing is similar to that observed on open beaches. In this case the circulation of the overall embayment was classified as "normal". The flow patterns as well as the bar and rip morphologies, which are obtained starting from highly idealized embayed beach geometries, are consistent with the observations provided in Fig. 1.

We showed that wave shadowing leads to smaller wave height against the headlands (Fig. 6a) when not overwhelmed by wave refraction in the case of significantly curved embayed beaches (Fig. 6f). Accordingly, wave height patterns, and in turn the presence of headland rips, are influenced by the characteristics of the directional spreading imposed at the seaward boundary. Fig. 9 shows the wave patterns and resulting wave-driven circulation at $t=0$ for an alongshore-uniform embayed beach with $L=500$ m and waves with $H_s=1$ m, $T_p=10$ s, $\theta=5^\circ$, considering a range of directional spreadings from 4° to 37.5°. Simulations show that wave shadowing increases with increasing directional spreading. This suggests that, for a given headland geometry, the presence of headland rips is favoured by waves with large directional spreading. For curved embayed beaches, there is a competition between wave shadowing due to the headlands and wave refraction due to the bathymetry. The balance between the two processes controls the eventual presence of headland rips. For instance, under wave forcing characterized by a directional spreading of 37.5° and a curved beach characterized by $L=1000$ m, wave shadowing becomes the dominant factor and results in the generation of headland rips. This is in contrast with the simulations performed over the same bathymetry but with a directional spreading of 8° as in this case only a central rip developed (not shown). Additional simulations including the effect of wave diffraction (not shown here) indicate that wave

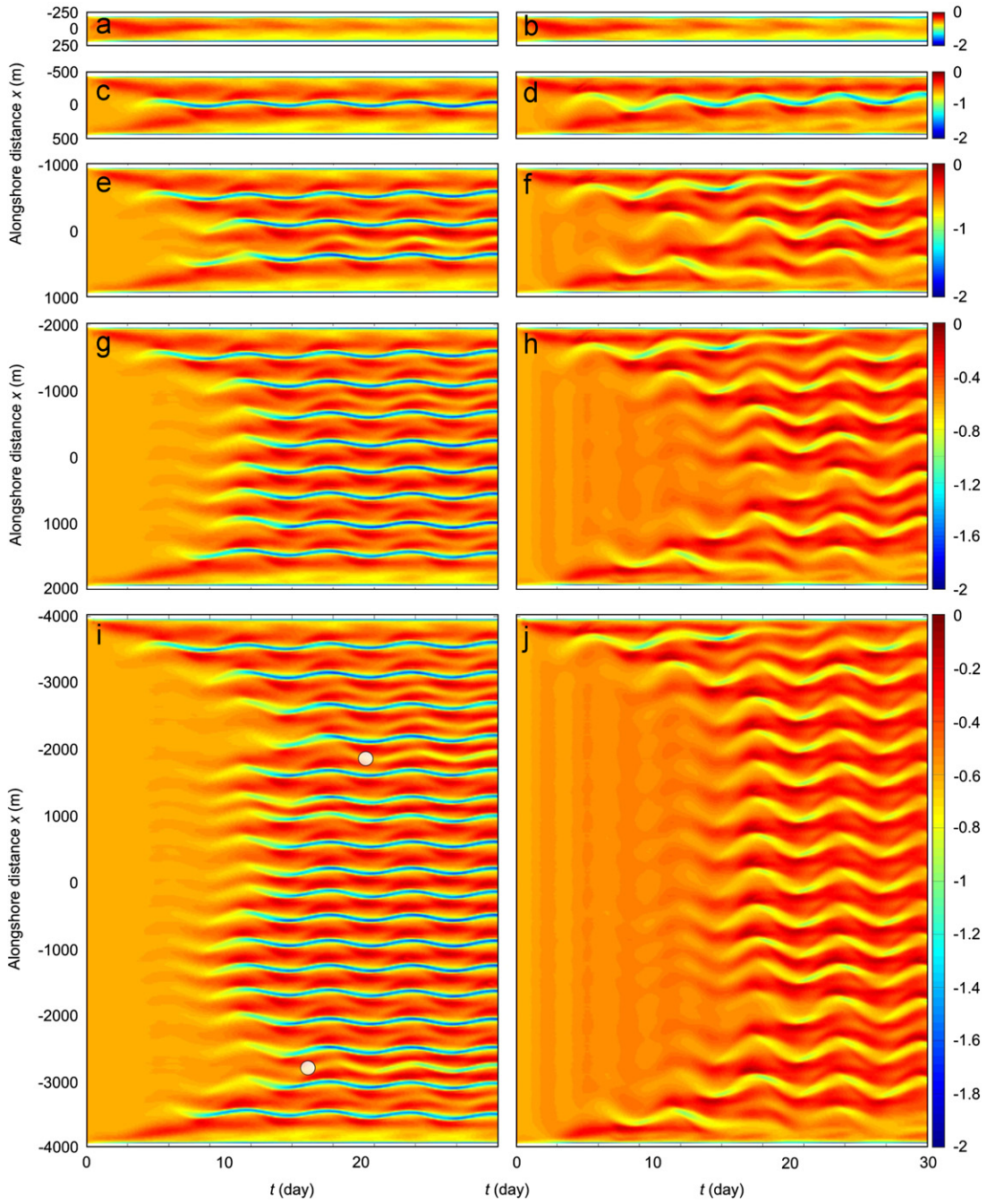

Fig. 7. Time evolution of the alongshore profile Z_b starting from an alongshore-uniform embayed beach and for $H_s=1$ m, $T_p=10$ s and time-varying wave angle θ with an amplitude (left-hand panels) $A=5^\circ$ and (left-hand panels) $A=10^\circ$. (a,b) $L=500$ m, (c,d) $L=1000$ m, (e,f) $L=2000$ m, (g,h) $L=4000$ m and (i,j) $L=8000$ m. In panel i the two white circles indicate the onset of splitting of shoal.

shadowing systematically overwhelms wave diffraction for both narrow banded swells and waves with large directional spreading. Overall, wave shadowing and the resulting alongshore gradients in wave height are the major driving mechanism for headland rips.

Table 1, listing the existing observations of embayed beach circulations with corresponding embayment parameter δ, shows that cellular circulation is generally observed for $\delta \leq 9$, transitional circulation for $9 < \delta < 16$ and normal circulation for $\delta \geq 16$. Fig. 10 synthesized our numerical experiments in terms of embayment parameter δ and λ. In our simulations with $\delta \leq 9$ (i.e., $\delta = 7.3$ for $L=500$ m), cellular beach circulation is always observed and is characterized by either cellular circulation with headland rips (Fig. 8a) or cellular circulation with a rip at the centre (Fig. 8b). Our simulations indicate that this result is not dependent on the wave angle. Accordingly, λ essentially depends on whether one central rip or two headland rips are observed (Fig. 10). For larger beach lengths ($\delta > 9$), beach circulation is influenced by both wave incidence and beach curvature. For shore-normal waves and initially alongshore-uniform embayed beaches, our numerical results are essentially similar to the observations in Table 1 as for $9 < \delta < 16$ (i.e., $\delta = 14.6$ for $L=1000$ m) and $\delta \geq 16$ ($L \geq 2000$ m), transitional and normal circulations are observed. For initially alongshore-uniform embayed beaches, the constant rip spacing $\lambda \approx 350$ m for $\delta > 16$ (Fig. 10) confirms that, for shore-normal waves, the presence of headlands does not impact the overall rip channel behaviour. This corresponds to configurations

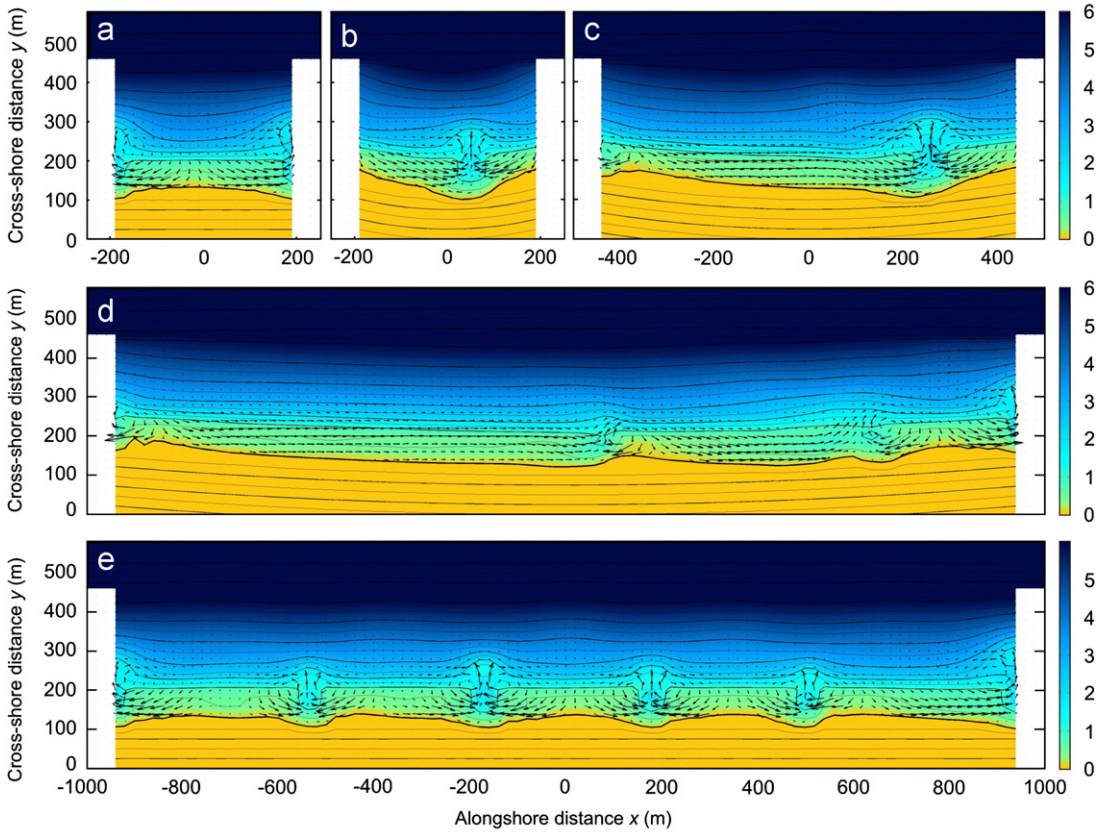

Fig. 8. Surfzone circulation and rip channel configurations: (a) Cellular circulation with headland rips. Simulation starting with an alongshore-uniform embayed beach (L=500 m and $\theta=5^{\circ}$) ; (b) Cellular circulation with a rip developing in the centre of the beach. Simulation starting with a curved embayed beach (L=500 m and $\theta=5^{\circ}$); (c) Asymmetric and transitional configuration with a rip channel/current occurring only at one end of the embayment (the updrift one). Simulation starting with a curved embayed beach (L=500 m and $\theta=5^{\circ}$); (d) Transitional circulation with a rip channel/current occurring at both ends of the embayment and two additional rips along the beach. Simulation starting with a curved embayed beach (L=2000 m and $\theta=5^{\circ}$); (e) Normal circulation with a rip channel/current occurring at both ends of the embayment and four additional rips along the beach. Simulation starting with an alongshore-uniform embayed beach (L=2000 m and $\theta=0^{\circ}$). All morphological configurations at t=10 days.

with a number of rips within the embayment larger than or equal to 4. This is more complicated for curved beaches as for $\delta=14.6$ ($L=1000$ m) and $\delta=29.2$ ($L=2000$ m), cellular circulation (with a central rip) and transitional circulation (3 rip channels along the beach) can be simulated, respectively. This suggests that the threshold values (9 and 16) in δ and the arbitrary threshold of 4 rips within the embayment could increase for increasing beach curvature. The same effect is obtained when the wave angle is changed (threshold values in δ increase with increasing θ and increasing variability in θ) and is the reason for the large variability in rip spacing for simulations characterized by $\delta>20$.

Our embayment parameter δ is slightly different from that (δ') proposed in Short and Masselink (1999). For embayed beaches where the headland length is larger than the typical surfzone width, the degree of embaymentisation predicted by δ' is systematically overestimated which is not the case with δ. We showed that in our simulations with shore-normal waves and initially alongshore-uniform embayed beaches, the degree of embayment predicted by δ is consistent with observations (Table 1). Yet, beach curvature and prevailing wave angle should be accounted for in δ to more accurately predict beach circulation. To some extent, δ should also account for the geometry of the headlands as, together with directional spreading, it controls the presence of headland rip and the dimensions of the shadowed region along the beach.

The impact of the headlands on beach circulation for high wave obliquity or time-varying wave angle to the shore can be addressed in more detail. For time-invariant oblique waves on an embayed beach with $L\leq 2000$ m, rip spacing systematically decreases with increasing distance from the updrift headland. The driving mechanism for the larger downdrift rip spacing is similar to the one described in Castelle et al. (2012) where it was shown that, for a given alongshore perturbation in the wave forcing (here the shadow region at the updrift headland), rip spacing immediately downdrift is larger than without a perturbation. This effect cascades to the following 3-4 downdrift rip channels with the rip spacing progressively decreasing and going back to the same value associated to the situation without a perturbation. This behaviour is exacerbated on curved embayed beaches as a result of the decreasing breaking wave angle to the shore with increasing distance to the updrift headland. Additionally, time varying θ results in persistent merging of free rips to headland rips, the onset of splitting of shoals, an increase in merging of rip channels and more alongshore-variable rip spacing. Similar conclusions were drawn in Castelle and Ruessink (2011) on open beaches. On embayed beaches, rip channel nonlinear behaviour is strengthened by the presence of the headlands as under time-varying wave conditions rip channels that are located in the vicinity of a headland systematically migrate towards and eventually merge with the headland rip. This in turn results in the onset of splitting of the nearby shoals. This effect can potentially cascade further along the embayment (e.g., Fig. 7h) ultimately resulting in different mean rip spacing than for the time-invariant shore-normal wave simulation (Fig. 10).

Simulations with high wave obliquity often resulted in the onset of beach rotation by the end of the 60-day simulation.

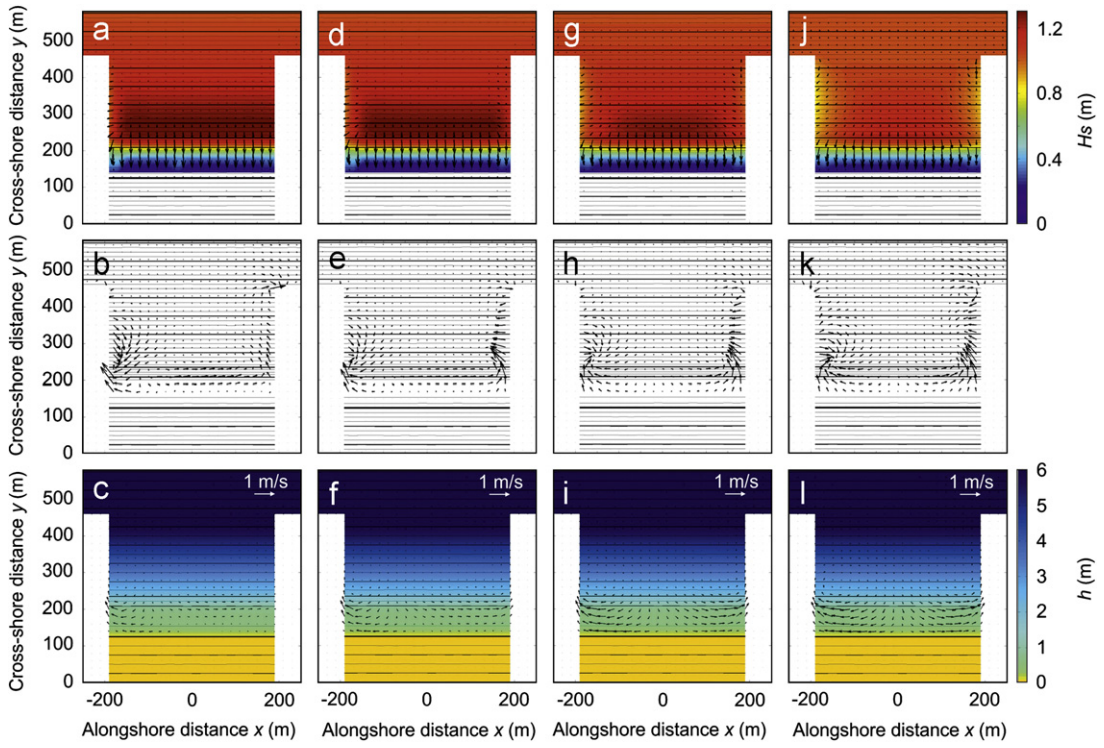

Fig. 9. Hydrodynamics at $t=0$ starting from an embayed beach with $L=500$ m and an alongshore-uniform shape, for offshore waves with $H_s=1$ m, $T_p=10$ s, $\theta=5^\circ$ with a direction spreading of (a,b,c) 4°, (d,e,f) 8° (used throughout the study), (g,h,i) 22.7° and (j,k,l) 37.5°. (a,d,g,j) Wave field with colour bar indicating significant wave height H_s in meters and resulting gradients in radiation stress $\vec{F}_w$ (arrows) with $F_{wi}=-(1/\rho)\partial S_{ij}/\partial x_j$. (b,e,h,k) Residual forcing $\vec{F}_r=\vec{F}_p+\vec{F}_w$ (arrows). (c,f,i,j) Resulting wave-driven circulation with colour bar indicating water depth in meters. In all panels iso-contours (0.5-m intervals) are contoured in the background.

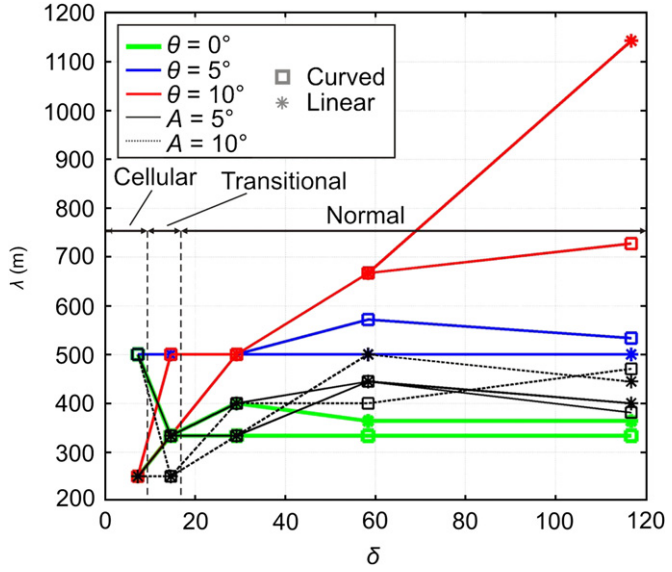

Fig. 10. λ versus the non-dimensional embayment scaling parameter δ. Simulations for $\theta=0^\circ$ are shown in green, $\theta=5^\circ$ in blue, $\theta=10^\circ$ in red, time-varying θ with $A=5^\circ$ in black and time-varying θ with $A=10^\circ$ with the dashed black line. Crosses and squares indicate simulations starting from an alongshore-uniform and a curved embayed beach, respectively. The two vertical dashed lines distinguish the cellular, transitional and normal embayed beach circulations deduced from the observations given in Table 1. (For interpretation of the references to color in this figure caption, the reader is referred to the web version of this article.)

Overall, beach rotation was favoured by large θ and embayed beach length of 1000 m $\leq L \leq$ 4000 m. The shoreline signal was dominated by the megacusps for shorter beach lengths (e.g., $L=500$ m) while longer embayed beaches (e.g., $L=8000$ m) would likely require more time to rotate significantly because of the larger amount of sand that needs to be transported from one side of the beach to the other, and because in this study we do not consider extreme storms but rather low- to moderate-energy conditions that imply a slow transport of sand from the updrift to the downdrift part of the beach. Fig. 11 shows a typical example of beach morphology at $t=60$ days for a simulation with time-invariant waves with $H_s=1$ m, $T_p=10$ s and $\theta=10^\circ$ starting from an alongshore-uniform embayed beach with $L=2000$ m. The simulated morphology shows that beach rotation is a dominant feature as most of the iso-contours rotated to the point that headland bypassing can also be observed. An emerged shoal is observed at $x\approx800$ m and $y\approx200$ m which coincides with the basic state bar crest. Since the down-slope transport depends on the bottom perturbation and beach rotation is not interpreted as a rotation of the basic state, resulting sediment transport fluxes can become unrealistic. In addition, recent observations suggest that cross-shore transport, which is not explicitly considered in the basic state approach, can dominate beach the rotation signal (Harley et al., 2011). Therefore, long-term ($t>20$ days) simulations of rip channel morphodynamics were disregarded in this paper and the role of migrating rip channels on beach rotation signal was not investigated.

The numerical model used in this study relies on a number of simplifying assumptions. These assumptions, which are discussed in more detail in Castelle and Ruessink (2011) are: disregard of both the wave group-scale forcing that is known to influence rip spacing (Reniers et al., 2004) and resolution of the vertical structure of the flow, despite the potentially significant variation of the velocity profile in rip currents (e.g., Haas and Svendsen, 2002). These are the typical assumptions in nonlinear morphodynamic modelling of 3D surfzone sandbars (e.g., Garnier et al.,

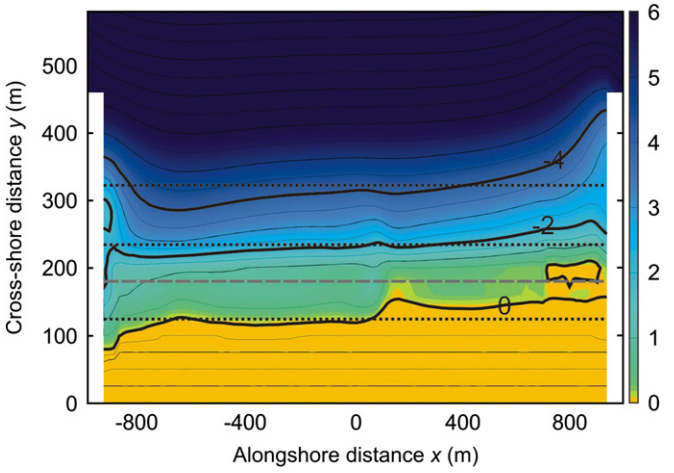

Fig. 11. Embayed beach bathymetry at $t=60$ days for a simulation starting from an alongshore-uniform embayed beach with $L=2000$ m with time-invariant waves with $H_s=1$ m, $T_p=10$ s and $\theta=10^{\circ}$. The thick black lines indicate respresentative iso-contours of the bathymetry with the thick dotted black line indicating the corresponding iso-contours at $t=0$. The thick dotted gray line shows the location of the basic state bar crest and the colour bar indicates seabed elevation in meters. The cross-shore scale is enlarged by a factor of 3.

2006). High curvatures in the planar beach shape were not addressed as large shoreline gradients in the vicinity of the headlands tend to result in numerical instabilities. The details of the shape of the headlands can control the presence and characteristics of rips developing in their proximity while in this study only one regular and simplified headland geometry and length has been considered. Wave diffraction, which is included in an approximate manner in SWAN, wave reflection and breaking against the headlands were not addressed in detail in this paper. Finally, the influence of changes in the flow circulation resulting from different values of H_s has not been addressed but will constitute the topic of a future study. Despite the number of model limitations, the considerable longshore variability of rip channel wavelength simulated on embayed beaches is consistent with the hypothesis that rips are self-organized patterns and is in line with recent field observations (Gallop et al., 2011) and the earlier pioneer work of Reniers et al. (2004).

Overall, the numerical model was capable of reproducing the main rip channel behaviour commonly observed on embayed beaches and the main beach circulation patterns. Simulations show that wave angle and the embayment size are crucial to rip channel morphodynamics on embayed beaches. Future observations on embayed beaches of large-scale rip channel behaviour and detailed field observations are needed to further improve the link between numerical models and reality, and to refine the embayment parameter δ. This will improve our skill to predict the characteristics of this critical and hazardous element of the nearshore system.

Acknowledgments

This work was done within the framework of the project BARBEC (ANR N2010 JCJC 602 01). GC acknowledges funding from NIWA (through NZ FRST) and Cantabria Campus International (Augusto Gonzalez Linares Program). The authors thank both Dr. A.D. Short and Dr. R.W. Brander for kindly providing the fantastic pictures of embayed beach rips shown in Fig. 1. Thanks to B.B. Lopez for prereviewing an earlier version of this manuscript and the reviewers for their constructive comments.

References

Bailard, J.A., 1981. An energetics total load sediment transport model for a plane beach. Journal of Geophysical Research 86 (C11), 10938–10954.
Battjes, J.A., 1975. Modelling of turbulence in the surfzone. In: Proceedings of Symposium on Modelling Techniques, ASCE, pp. 1050–1061.
Battjes, J.A., Stive, M.J.F., 1985. Calibration and verification of a dissipation model for random breaking waves. Journal of Geophysical Research 90 (C5), 9159–9167.
Bonneton, P., Bruneau, N., Castelle, B., Marche, F., 2010. Large-scale vorticity generation due to dissipating waves in the surf zone. Discrete and Continuous Dynamical Systems - Series B 13 (4), 729–738.
Booij, N., Ris, R.C., Holthuijsen, L.H., 1999. A third-generation wave model for coastal regions, Part 1, Model description and validation. Journal of Geophysical Research 104 (C4), 7649–7666.
Bruneau, N., Bonneton, P., Castelle, B., Pedreros, R., 2011. Modeling rip current circulations and vorticity in a high-energy meso-macrotidal environment. Journal of Geophysical Research 116 (C07026), http://dx.doi.org/10.1029/2010JC006693.
Calvete, D., Dodd, N., Falqués, A., Van Leeuwen, S.M., 2005. Morphological development of rip channel systems: normal and near-normal wave incidence. Journal of Geophysical Research 110 (C10006), http://dx.doi.org/10.1029/2004JC002803.
Castelle, B., Bonneton, P., 2006. Modelling of a rip current induced by waves over a ridge and runnel system on the Aquitanian Coast, France. Comptes Rendus Geoscience 338, 711–717.
Castelle, B., Marieu, V., Coco, G., Bonneton, P., Bruneau, N., Ruessink, B.G., 2012. On the impact of an offshore bathymetric anomaly on surfzone rip channels. Journal of Geophysical Research 117 (F01038), http://dx.doi.org/10.1029/2011JF002141.
Castelle, B., Ruessink, B.G., 2011. Modeling formation and subsequent nonlinear evolution of rip channels: time-varying versus time-invariant wave forcing. Journal of Geophysical Research 116 (F04008), http://dx.doi.org/10.1029/2011JF001997.
Castelle, B., Ruessink, B.G., Bonneton, P., Marieu, V., Bruneau, N., Price, T.D., 2010. Coupling mechanisms in double sandbar systems, Part 1: Patterns and physical explanation. Earth Surface Processes and Landforms 35, 476–486.
Coco, G., Murray, A.B., 2007. Patterns in the sand: from forcing templates to self-organization. Geomorphology 91, 271–290.
Dalrymple, R.A., MacMahan, J.H., Reniers, A.J.H.M., Nelko, V., 2011. Rip currents. Annual Review of Fluid Mechanics 43, 551–581.
Daly, C.J., Bryan, K.R., Roelvink, J.A., Klein, A.H.F., Hebbeln, D., Winter, C., 2011. Morphodynamics of embayed beaches: the effect of wave conditions. Journal of Coastal Research SI 64, 1003–1007.
Deigaard, R., Drønen, N., Fredsøe, J., Jensen, J.H., Jørgensen, M.P., 1999. A morphological stability analysis for a long straight barred coast. Coastal Engineering 36, 171–195.
Enjalbert, C., Castelle, B., Rihouey, D., Dailloux, D., 2011. High-frequency video observation of geologically-constrained barred-beach: La Grande Plage de Biarritz (France). Journal of Coastal Research SI 64, 70–74.
Falqués, A., Coco, G., Huntley, D.A., 2000. A mechanism for the generation of wave-driven rhythmic patterns in the surf zone. Journal of Geophysical Research 105, 24071–24088.
Gallop, S.L., Bryan, K.R., Coco, G., Stephens, S.A., 2011. Storm-driven changes in rip channel patterns on an embayed beach. Geomorphology 127, 179–188.
Garnier, R., Calvete, D., Falqués, A., Caballeria, M., 2006. Generation and nonlinear evolution of shore-oblique/transverse sand bars. Journal of Fluid Mechanics 567, 327–360.
Garnier, R., Calvete, D., Falqués, A., Dodd, N., 2008. Modelling the formation and the long-term behavior of rip channel systems from the deformation of a longshore bar. Journal of Geophysical Research 113 (C07053), http://dx.doi.org/10.1029/2007JC004632.
Haas, K.A., Svendsen, I.A., 2002. Laboratory measurements of the vertical structure of rip currents. Journal of Geophysical Research 107 (C5), 5–11, http://dx.doi.org/10.1029/2001JC000911.
Haas, K.A., Svendsen, I.A., Brander, R.W., Nielsen, P., 2002. Modeling of a rip current system on Moreton Island, Australia. In: Proceedings of 28th International Conference on Coastal Engineering, vol. 1, ASCE, New York, pp. 784–796.
Harley, M.D., Turner, I.L., Short, A.D., Ranasinghe, R., 2011. A reevaluation of coastal embayment rotation: the dominance of cross-shore versus alongshore sediment transport processes, Collaroy-Narrabeen Beach, southeast Australia. Journal of Geophysical Research 116 (F04033), http://dx.doi.org/10.1029/2010JF001989.
Holman, R.A., Symonds, G., Thornton, E.B., Ranasinghe, R., 2006. Rip spacing and persistence on an embayed beach. Journal of Geophysical Research 111 (C06006), http://dx.doi.org/10.1029/2005JC002965.
Hsu, J.R.C., Silvester, R., Xia, Y.M., 1989. Generalities on static equilibrium bays. Coastal Engineering 12, 353–369.
Huntley, D.A., Hendry, M.D., Haines, J., Greenidge, B., 1988. Waves and rip currents on a Caribbean pocket beach, Jamaica. Journal of Coastal Research 4, 69–79.
Jackson, D.W.T., Cooper, J.A.G., Rio, L.D., 2005. Geological control of beach morphodynamic state. Marine Geology 216, 297–314.
Klein, A.H.F., Ferreira, O., Dias, J.M.A., Tessler, M.G., Silveira, L.F., Benedet, L., de Menezes, J.T., de Abreu, J.G.N., 2010. Morphodynamics of structurally controlled headland-bay beaches in southeastern Brazil: a review. Coastal Engineering 57, 98–111.

Komar, P.D., Allan, J.C., Dias-Mendez, G.M., Marra, J.J., Ruggiero, P., 2000. El Niño and La Niña: erosion processes and impacts. In: 27th International Conference on Coastal Engineering, ASCE, pp. 2414–2427.
Loureiro, C., Ferreira, O., Cooper, J.A.G., 2012. Extreme erosion on high-energy embayed beaches: influence of megarips and storm grouping. Geomorphology 139–140, 155–171.
MacMahan, J.H., Thornton, E.B., Reniers, A.J.H.M., 2006. Rip current review. Coastal Engineering 53, 191–208.
McNinch, J.E., 2004. Geologic control in the nearshore: shore-oblique sandbars and shoreline erosion hotspots, Mid-Atlantic Bight, USA. Marine Geology 211, 121–141.
Mei, C.C., 1989. Applied Dynamics of Ocean Waves. World Scientific.
Ojeda, E., Guillen, J., 2008. Shoreline dynamics and beach rotation of artificial embayed beaches. Marine Geology 253, 51–62.
Ojeda, E., Guillen, J., Ribas, F., 2011. Dynamics of single-barred embayed beaches. Marine Geology 280, 76–90.
Philipps, O.M., 1977. The dynamics of the upper ocean. Cambridge University Press.
Ranasinghe, R., McLoughlin, R., Short, A.D., Symonds, G., 2004. The Southern Oscillation Index, wave climate, and beach rotation. Marine Geology 204, 273–287.
Reniers, A.J.H.M., Roelvink, J.A., Thornton, E.B., 2004. Morphodynamic modeling of an embayed beach under wave group forcing. Journal of Geophysical Research 109 (C01030), http://dx.doi.org/10.1029/2002JC001586.
Ribas, F., Garnier, R., Ojeda, E., Falqués, A., Guillén, J., Calvete, D., 2007. Observation and modeling of crescentic bars in Barcelona embayed beaches. In: Proceedings of Coastal Sediments '07, ASCE.
Ruessink, B.G., Coco, G., Ranasinghe, R., Turner, I.L., 2007. Coupled and noncoupled behavior of three-dimensional morphological patterns in a double sandbar system. Journal of Geophysical Research 112 (C07002), http://dx.doi.org/10.1029/2006JC003799.
Schyuer-Ming, S., Komar, P.D., 1994. Sediments, beach morphology and seacliff erosion within an Oregon Coast littoral cell. Journal of Coastal Research 10, 144–157.
Scott, T.M., Masselink, G., Russell, P.E., 2011. Morphodynamic characteristics and classification of beaches in England and Wales. Marine Geology 286, 1–20.
Scott, T.M., Russell, P.E., Masselink, G., Woolers, A., Short, A.D., 2007. Beach rescue statistics and their relation to nearshore morphology and hazards: a case study for southwest England. Journal of Coastal Research SI 50, 1–6.
Short, A.D., 2006. Australian beach systems—nature and distribution. Journal of Coastal Research 22, 11–27.
Short, A.D., Masselink, G., 1999. Embayed and structurally controlled embayed beaches. In: Short, A.D. (Ed.), Handbook of Beach and Shoreface Morphodynamics. Wiley, Chichester, pp. 230–250.
Silva, R., Baquerizo, A., Losada, M.A., Mendoza, E., 2010. Hydrodynamics of headland-bay beach-nearshore current circulation. Coastal Engineering 57, 160–175.
Silvester, R., 1960. Stabilization of sedimentary coastlines. Nature 188, 467–469.
Smit, M.W.J., Reniers, A.J.H.M., Ruessink, B.G., Roelvink, J.A., 2008. The morphological response of a nearshore double sandbar system to constant wave forcing. Coastal Engineering 55, 761–770.
Splinter, K.D., Holman, R.A., Plant, N.G., 2011. A behavior-oriented dynamic model for sand bar migration and 2DH evolution. Journal of Geophysical Research 116.
Van Enckevort, I.M.J., Ruessink, B.G., Coco, G., Susuki, K., Turner, I.L., Plant, N.G., Holman, R.A., 2004. Observations of nearshore crescentic sandbars. Journal of Geophysical Research 109 (C06028), http://dx.doi.org/10.1029/2003JC002214.
Wright, L.D., Short, A.D., 1984. Morphodynamic variability of surf zones and beaches: a synthesis. Marine Geology 56, 93–118.
Yamashita, T., Tsuchiya, Y., 1992. Numerical simulation of pocket beach formation. In: Proceedings of 23rd International Conference on Coastal Engineering, ASCE, New York, pp. 2556–2566.